A theoretical study of the effects of uniaxial stress and spatial dielectric functions on the density of states of shallow donor impurities in a GaAs quantum well dot of circular geometry

F. Oketch[a,*] and H. Oyoko[b]

[a]*Department of Mathematics and Physics, Technical University of Mombasa, Mombasa 90420-80100, Kenya*
[*]*e-mail: fomboga@tum.ac.ke*
[b]*Department of Physics, Pwani University, Kilifi 195-80108, Kenya.*

Received 4 September 2023; accepted 2 October 2023

In the present work, we have carried out a comparative study of the effects of uniaxial stress and spatial dielectric functions on the density of impurity states (DOIS) of shallow donor impurities ina GaAs quantum well dot of circular cross-section. Using a trial wave function in the effective mass approximation, we carried out calculations for a range of binding energies of hydrogenic (dielectric constant) and non-hydrogenic (spatial dielectric functions) donors for various applied uniaxial stress and for different uniaxial lengths of the quantum dot. Our results show that, for a constant axial length of the quantum dot and constant uniaxial stress, the DOIS for the donor impurity is markedly enhanced for the non-hydrogenic donor impurity over that for purely hydrogenic donor impurity. At constant axial length, the applied uniaxial stress enhances the DOIS in both cases. The density of impurity states has also been studied for a constant applied uniaxial stress for different axial lengths of the quantum dot. Here, again, the DOIS increases with increasing axial length of the quantum dot. In fact, the enhanced DOIS is observed throughout the range of binding energies considered. These results show that not only does the DOIS vary with the applied uniaxial stress and spatial dielectric functions they are also different for various axial lengths of the quantum dot. These findings indicate that it is important to take into account the effect of applied uniaxial stress and spatial dielectric functions when performing experimental studies of electronic, optical and transport properties of such nanostructures as quantum dots.

Keywords: Density of impurity states; GaAs quantum well dot; spatial dielectric function; applied uniaxial stress.

DOI: https://doi.org/10.31349/RevMexFis.70.030501

1. Introduction

When impurities such as hydrogenic and non-hydrogenic donors are introduced into semiconductors, they affect carrier transport and optical properties of such semiconductors. This is because they introduce bound states in the forbidden gap of such materials [1]. For more than three decades, a number of theoretical and experimental studies have been carried out on various effects of these donor impurities in semiconductor nanostructures such as quantum wells (QWs), quantum well wires (QWWs) and quantum dots (QDs) [2-9]. These studies have considered the donor and acceptor impurity binding energies and density of impurity states (DOIS) in various geometries of the above-mentioned nanostructures. The hydrostatic pressure, uniaxial stress, and electric field effects, in the low temperature regime (close to 4 K), have been reported for donor impurities in single QWs [10-12], symmetrical and asymmetrical double quantum wells (DQW) [13,14], QWWs [15,16] and GaAs QDs [17-19]. As a general feature, the studies show that the binding energy of a donor electron is enhanced by increasing the hydrostatic pressure and the uniaxial stress. H. Oyoko [20] used a variational technique to calculate the binding energy of a hydrogenic donor impurity using a dielectric constant and that of a non-hydrogenic donor impurity using the Hermanson's spatial dielectric function in the Coulomb potential. The donor impurity, in this case, was embedded in a GaAs QWW of circular cross-section. The author found that the effect of the Hermanson's spatial dielectric function is to increase the donor impurity binding energy with decreasing QWW radius over that of the hydrogenic donor impurity.

In the present work, we have carried out a comparative theoretical study of the effect of Thomas- Fermi and Hermanson's spatial dielectric functions and applied uniaxial stress on the density of impurity states of a donor impurity ina GaAs quantum dot of cylindrical cross section. In the study, we calculated the donor impurity binding energies as functions three different dielectric functions and applied uniaxial stress. We then computed the DOIS of the donor impurity as a function of the binding energies. In our calculations we have used a variational technique in the effective mass and dipole approximation [21-24]. We have assumed that $\mathrm{Ga}_{1-x}\mathrm{Al}_x\mathrm{As}$ matrix surrounding the GaAs quantum dot (QD) provides an infinite potential barrier due to the large band gap between the two [6].

Our work is organized as follows: In Sec. 2, we present the theoretical framework, while in Sec. 3, we present the results and discussions. Finally, in Sec. 4, we give our conclusions.

2. Theoretical model

2.1. Hydrogenic donor impurity

The Hamiltonian for a 1s hydrogenic donor impurity which is located at the center of a cylindrical QD is given by

$$H_h = -\frac{\hbar^2}{2m_{d,b}{}^*(P)}\left(\frac{1}{\rho}\frac{\partial}{\partial\rho}\left[\rho\frac{\partial}{\partial\rho}\right]+\frac{\partial^2}{\partial \boldsymbol{z}^2}\right) - \frac{e^2}{4\pi\varepsilon_{d,b}(P)r}+V_B(r,P), \quad (1)$$

where $m^*(P)$ and $\varepsilon_{d,b}(P)$ are the uniaxial stress dependent effective mass of the donor impurity in the QD and uniaxial stress dependent dielectric function of the GaAs, respectively. The two subscripts d and b refer to the quantum well dot and the barrier layer materials, respectively while r, represents the position of the donor impurity and is expressed as $r = [\rho^2 + \boldsymbol{z}^2]^{1/2}$.

In Eq. (1), the stress dependent effective mass for the donor impurity in the quantum dot material is determined from the expression [25-27],

$$m_d^*(T) = \left(1 + E_P^\Gamma(P)\left[\frac{2}{E_g^\Gamma(P)} + \{E_g^\Gamma(P)+\Delta_0\}^{-1}\right]\right)^{-1} m_e, \quad (2)$$

where m_e, is the free electron mass, $E_g^\Gamma(P) = 7.51$ eV is the energy related to the momentum matrix element, $\Delta_0 = 0.341$ eV is the spin-orbit splitting. $E_g^\Gamma(P)$ is the stress dependent energy gap for the GaAs QD semiconductor at the Γ-point in units of eV [28],

$$E_g^\Gamma(P) = a + bP + cP^2, \quad (3)$$

where $a = 1.425$ eV, $b = 1.26 \times 10^{-2}$ eV/kbar, $c = -3.77 \times 10^{-5}$ eV/(kbar)^2 and $E_g^\Gamma(0) = 1.519$ eV is the energy gap for GaAs quantum dot at the Γ-point when the uniaxial stress is $P = 0$ kbar. The expression for determining the barrier material's parabolic conduction effective mass as a function of uniaxial stress is [25-27]:

$$m_b^*(P) = m_d^*(P) + 0.083x, \quad (4)$$

where $x = 0.3$ is the mole fraction of Aluminum in the $Ga_{1-x}Al_xAs$ layer. In the GaAs quantum dot region the stress dependent dielectric function, $\varepsilon_d(P)$ is given by [25-27]

$$\varepsilon_d(P) = \varepsilon_d(0)\exp(\delta P), \quad (5)$$

where $\varepsilon_d(0) = 12.56$ [6] is the static dielectric constant for GaAs and $\delta = -1.73 \times 10^{-3}$ kbar^{-1}.

The static dielectric constant of the barrier material, obtained from a linear interpolation of the dielectric constants of GaAs and $Ga_{1-x}Al_xAs$ is given by

$$\varepsilon_b(P) = \varepsilon_d(P) - 3.12x. \quad (6)$$

In Eq. (1)

$$V_B(z,P) = \begin{cases} 0, & \text{for} \quad |z| \leq \frac{L_z(P)}{2} \\ V_0(P), & \text{for} \quad |z| \geq \frac{L_z(P)}{2} \end{cases}, \quad (7)$$

is the barrier potential which confines the donor impurity within the quantum dot. In this equation, $L_z(P)$ is the stress-dependent length of the QD and $V_0(P)$ is the barrier height expressed as a function of the uniaxial stress P. These are given by,

$$L_z(P) = L_z(0)[1 - \{S_{11} + 2S_{12}\}P], \quad (8)$$

and

$$V_0(P) = Q_c \Delta E_g^\Gamma(x,P), \quad (9)$$

where in Eq. (7), $S_{11} = 1.16 \times 10^{-3}$ kbar^{-1} and $S_{12} = -3.7 \times 10^4$ kbar^{-1} and $L_z(0)$ is the unstrained length of the QD. In Eq. (9), $Q_c = 0.658$ is the band offset parameter, while $\Delta E_g^\Gamma(x,P)$ is the band gap difference between the quantum dot material and the barrier layer material as a function of the stress and aluminum concentration x, and is expressed as

$$\Delta E_g^\Gamma(x,P) = \Delta E_g^\Gamma(x) + PD(x). \quad (10)$$

The quantity $\Delta E_g^\Gamma(x)$ is the stress-independent variation of the energy gap difference and is given by $\Delta E_g^\Gamma(x) = (1.155x + 0.37x^2)$ eV. The quantity $D(x)$ is defined as the uniaxial stress coefficient of the band gap difference and is given by

$$D(x) = \left(-[1.3 \times 10^{-3}]x\right) \quad \text{eV/kbar}. \quad (11)$$

Our trial wave function for the hydrogenic donor impurity in its ground state is given by

$$\Psi_{1S}(\rho,\boldsymbol{z}) = N_{1S} J_0(k_{10}\rho)\cos(\beta z) \times \exp\left(-\lambda\left[\rho^2 + z^2\right]^{1/2}\right). \quad (12)$$

The normalization constant, N_{1S}, is given by

$$N_{1S} = \left(2\pi\int_0^d \rho J_0^2(k_{10}\rho)d\rho \times \int_0^{L_z/2} \cos^2(\beta z)\exp\left[-2\lambda\{\rho^2+z^2\}^{1/2}\right]dz\right)^{-1/2}.$$

The kinetic energy is determined as follows:

$$
\begin{aligned}
H_T\Psi_{1S}(\rho,z) &= -\frac{\hbar^2}{2m^*(P)}\left(\frac{1}{\rho}\frac{\partial}{\partial\rho}\left[\rho\frac{\partial}{\partial\rho}\right]+\frac{\partial^2}{\partial z^2}\right)\Psi_{1S}(\rho,z) = -\frac{\hbar^2}{2m^*(P)}\left(\frac{1}{\rho}\frac{\partial}{\partial\rho}\left[\rho\frac{\partial}{\partial\rho}\right]+\frac{\partial^2}{\partial z^2}\right)\\
&\times N_{1S}J_0(k_{10}\rho)\cos(\beta z)\exp\left(-\lambda\left[\rho^2+z^2\right]^{1/2}\right)\\
&= \frac{\hbar^2 N_{1S}}{2m^*(P)}(\alpha^2+\beta^2-\lambda^2)J_0(k_{10}\rho)\cos(\beta z)\exp\left(-\lambda[\rho^2+z^2]^{1/2}\right)+\frac{\lambda\hbar^2 N_{1S}}{m^*(P)}\\
&\times \frac{J_0(k_{10}\rho)\cos(\beta z)\exp\left(-\lambda\left[\rho^2+z^2\right]^{1/2}\right)}{(\rho^2+z^2)^{1/2}} - \frac{\lambda\rho\alpha\hbar^2 N_{1S}}{m^*(P)}\frac{J_1(k_{10}\rho)\cos(\beta z)\exp\left(-\lambda\left[\rho^2+z^2\right]^{1/2}\right)}{(\rho^2+z^2)^{1/2}}\\
&- \frac{\lambda z\beta\hbar^2 N_{1S}}{m^*(P)}\frac{J_0(k_{10}\rho)\sin(\beta z)\exp\left(-\lambda\left[\rho^2+z^2\right]^{1/2}\right)}{(\rho^2+z^2)^{1/2}},
\end{aligned}
\tag{13}
$$

where H_T is the kinetic energy part of the Hamiltonian given in Eq. (1). The kinetic energy of the donor impurity is thus obtained as,

$$
\begin{aligned}
T_h &= \int \Psi_{1S}{}^*(\rho,z)[H_T\Psi_{1S}(\rho,z)]dV = \frac{\hbar^2 N_{1S}^2(\alpha^2+\beta^2-\lambda^2)}{2m^*(P)} + \frac{\lambda\hbar^2 N_{1S}^2}{m^*(P)}\int_0^d \rho J_0^2(k_{10}\rho)d\rho\\
&\times \int_0^{L_z(P)/2}\frac{\cos^2(\beta z)\exp(-2\lambda[\rho^2+z^2]^{1/2})}{[\rho^2+z^2]^{1/2}}dz - \frac{\lambda\alpha\hbar^2 N_{1S}^2}{m^*(P)}\int_0^d \rho^2 J_1(k_{10}\rho)J_0(k_{10}\rho)d\rho\\
&\times \int_0^{L_z(P)/2}\frac{\cos^2(\beta z)\exp(-2\lambda[\rho^2+z^2]^{1/2})}{[\rho^2+z^2]}dz - \frac{\beta\lambda\hbar^2 N_{1S}^2}{m^*(P)}\int_0^d \rho J_0^2(k_{10}\rho)d\rho\\
&\times \int_0^{L_z(P)/2} z\frac{\cos(\beta z)\sin(\beta z)\exp(-2\lambda[\rho^2+z^2]^{1/2})}{[\rho^2+z^2]^{1/2}}dz.
\end{aligned}
\tag{14}
$$

The potential energy for the hydrogenic donor impurity is given by

$$
\begin{aligned}
V_\hbar(\rho,z) &= -\frac{e^2}{4\pi\varepsilon(0)}\int \Psi_{1S}^*(\rho,z)\left(\frac{1}{(\rho^2+z^2)^{1/2}}\Psi_{1S}(\rho,z)\right)dV = -\frac{e^2N_{1S}^2}{4\pi\varepsilon(0)}\int_0^{2\pi}d\varphi\int_0^d \rho J_0^2(k_{10}\rho)d\rho\\
&\times \int_0^{L_z/2}\frac{\cos^2(\beta z)\exp(-2\lambda[\rho^2+z^2]^{1/2})dz}{[\rho^2+z^2]^{1/2}} = -\frac{e^2N_{1S}^2}{2\varepsilon(0)}\\
&\times \int_0^d \rho J_0^2(k_{10}\rho)d\rho\int_0^{L_z/2}\frac{\cos^2(\beta z)\exp(-2\lambda[\rho^2+z^2]^{1/2})dz}{[\rho^2+z^2]^{1/2}}.
\end{aligned}
\tag{15}
$$

Thus, the total ground state energy of the donor impurity is given by

$$
E_{h,total}(P) = T_h + V_h. \tag{16}
$$

2.2. Total energy of the donor in the excited state

The Hamiltonian of the hydrogenic donor impurity in the final state to which it is excited is given by

$$
\begin{aligned}
H_f &= -\frac{\hbar^2}{2m^*(P)}\left(\frac{1}{\rho}\frac{\partial}{\partial\rho}\left[\rho\frac{\partial}{\partial\rho}\right]+\frac{\partial^2}{\partial z^2}\right)\\
&+ V_B(\rho,z,P).
\end{aligned}
\tag{17}
$$

The wave function for the donor impurity in this state is given by

$$\Psi_f(\rho, z) = N_f J_0(k_{10}\rho)\cos(\beta z)\exp(ikz), \tag{18}$$

where $k = 0$ in this state. Hence, the total energy of the donor impurity in this state is

$$E_f(P) = \frac{-\hbar^2}{2m^*(P)}\frac{\int \Psi_f^*[H_f \Psi_f]dV}{\int \Psi_f^* \Psi dV}, \tag{19}$$

where

$$\int \Psi_f^* \Psi_f dV = 1,$$

is the normalization condition. This yields the normalization constant as,

$$N_f^2 = \left(\int_0^{2\pi} d\phi \int_0^d \rho J_0^2(k_{10}\rho) \int_0^{L_z/2} \cos^2(\beta z)dz\right)^{-1}$$
$$= \left(2\pi \int_0^d \rho J_0^2(k_{10}\rho)d\rho \int_0^{L_z/2} \cos^2(\beta z)dz\right)^{-1}. \tag{20}$$

From Eqs. (17) and (18), the total energy of the excited state is found to be

$$E_f(P) = \frac{\hbar^2(\alpha^2 + \beta^2)}{m^*(P)}. \tag{21}$$

The minimum ground state energy, $E_{\min}$, of the donor impurity is obtained from the expression in Eq. (16), subject to the minimization condition

$$\frac{\partial E_{h,\text{total}}(P)}{\partial \lambda} = 0. \tag{22}$$

The binding energy of the donor impurity is then obtained from the Eqs. (15) and (20), thus,

$$E_b(P) = E_f(P) - E_{\min}(P). \tag{23}$$

2.3. A case of Linearized Thomas-Fermi and Hermansons' spatial dielectric functions

In this sub-section, the Hamiltonian for the donor impurity is given by

$$H' = -\frac{\hbar^2}{2m^*(P)}\left(\frac{1}{\rho}\frac{\partial}{\partial \rho}\left[\rho \frac{\partial}{\partial \rho}\right] + \frac{\partial^2}{\partial \boldsymbol{z}^2}\right) - \frac{e^2}{4\pi\varepsilon_d(\rho, \boldsymbol{z}, P)}\frac{1}{(\rho^2 + \boldsymbol{z}^2)^{1/2}} + V_B(\rho, \boldsymbol{z}, P), \tag{24}$$

with the stress-dependent spatial dielectric function given by

$$\varepsilon_d(\rho, \boldsymbol{z}, P) = \varepsilon_d(\rho, \boldsymbol{z})\exp(\delta P), \tag{25}$$

where $\delta = -1.73 \times 10^{-3}$ kbar^{-1}. $\varepsilon_d(\rho, \boldsymbol{z})$ is expressed as $\varepsilon_1(\rho, \boldsymbol{z})$ in the first instance, and in the second instance, as $\varepsilon_2(\rho, \boldsymbol{z})$. Here $\varepsilon_1(\rho, \boldsymbol{z})$, given by

$$\varepsilon_1(\rho, \boldsymbol{z}) = \varepsilon(0)\exp\left(-\mu\left[\rho^2 + \boldsymbol{z}^2\right]^{1/2}\right), \tag{26a}$$

is the linearized form of Thomas-Fermi screening function while $\varepsilon_2(\rho, \boldsymbol{z})$ is Hermanson's spatial dielectric function,

$$\frac{1}{\varepsilon_2(\rho, z)} = \frac{1}{\varepsilon(0)} + \left(1 - \frac{1}{\varepsilon(0)}\right) \times \exp\left(-\eta\left[\rho^2 + \boldsymbol{z}^2\right]^{1/2}\right). \tag{26b}$$

The static dielectric constant, $\varepsilon(0) = 12.56$ [6]. μ and η in Eqs. (26a) and (26b) respectively, are constants given as $\mu = 6.61 \times 10^{-2}$ nm while $\eta = 1.86 \times 10^2$ nm.

In the linearized Thomas-Fermi dielectric screening regime the expectation value of the potential energy operator in the Hamiltonian now becomes

$$\langle V_1(\rho, \boldsymbol{z})\rangle = -\frac{e^2}{4\pi}\int \Psi_{1S}^*(\rho, \boldsymbol{z}) \times \left(\frac{1}{\varepsilon_1(\rho, z)}\frac{1}{(\rho + z)^{1/2}}\Psi_{1S}(\rho, z)\right)dV$$
$$= -\frac{e^2 N_{1S}^2}{4\pi}\int_0^{2\pi} d\varphi \int_0^d \rho J_o^2(k_{10}\rho)d\rho \times \int_0^{L_z/2} \frac{1}{\varepsilon_1(\rho, z)}\cos^2(\beta z) \times \frac{\exp\left(-[2\lambda + \mu]\left[\rho^2 + z^2\right]^{1/2}\right)}{(\rho^2 + z^2)^{1/2}}dz$$
$$= -\frac{e^2 N_{1S}^2}{2}\int_0^d \rho J_o^2(k_{10}\rho)d\rho \int_0^{L_z/2} \cos^2(\beta z) \times \frac{\exp\left(-[2\lambda + \mu]\left[\rho^2 + z^2\right]^{1/2}\right)}{(\rho^2 + z^2)^{1/2}}dz, \tag{27}$$

while in the Hermanson's dielectric function regime the Hamiltonian for the donor impurity now has an additional term, ΔV, in the potential energy operator due to the spatial dielectric function $\varepsilon_2(\rho, z)$. We have used here also, the same trial wave function as for the Thomas-Fermi case. Thus,

$$V_2(\rho, z) = V_h + \Delta V, \tag{28}$$

where V_h, is given by Eq. (15) and ΔV is a perturbative term due the spatial dielectric function and is given by

$$\Delta V = -\frac{e^2}{4\pi}\left(1-\frac{1}{\varepsilon(0)}\right)N_h^2\int_0^{2\pi}d\phi\int_0^d \rho J_0^2(k_{10}\rho)d\rho\int_0^{L_z/2} \times \frac{\cos^2(\beta z)\exp\left(-[\eta+2\lambda][\rho^2+z^2]^{1/2}\right)}{(\rho^2+z^2)^{1/2}}dz,$$

or,

$$\Delta V = -\frac{e^2N_h^2}{2}\left(1-\frac{1}{\varepsilon(0)}\right)\int_0^d \rho J_0^2(k_{10}\rho)d\rho\int_0^{L_z/2} \times \frac{\cos^2(\beta z)\exp\left(-[\eta+2\lambda][\rho^2+z^2]^{1/2}\right)}{(\rho^2+z^2)^{1/2}}dz. \quad (29)$$

The total energy of the donor impurity is thus given by

$$E_{\text{total},2} = T_h + V_h + \Delta V. \quad (30)$$

2.4. Binding energy and density of impurity states

In all the above cases, the binding energy is obtained by subtracting the respective minimum energy from the corresponding free energy. The binding energy is then used to obtain the density of impurity states from [8].

$$g[E_b(P)] = \frac{1}{\pi R^2 L_z(P)}\int_{L_z[E_b-\text{Const}]}\frac{dL_z(P)}{|\Delta E_b(P)|}. \quad (31)$$

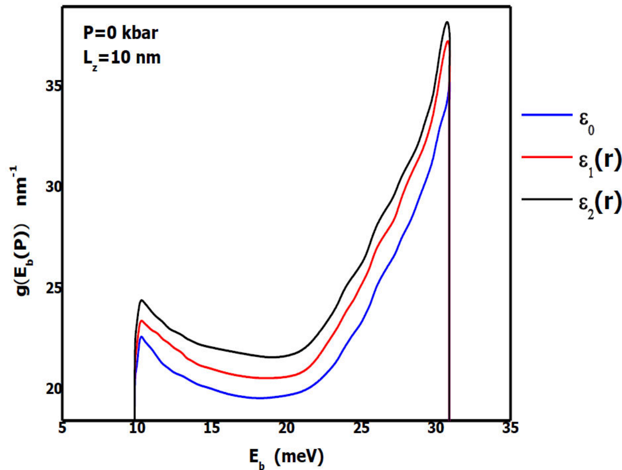

FIGURE 1. Density of impurity states (DOIS) of donor impurity in a cylindrical GaAs quantum well dot as a function of the donor binding energy at zero applied uniaxial stress, $P = 0$ kbar for the dot's width $L_z = 10$ nm. ε_0, represents DOIS when dielectric constant is used, $\varepsilon_1(r)$ represents DOIS with Linearized Thomas-Fermi dielectric function, while $\varepsilon_2(r)$ represents DOIS with the Hermanson's spatial dielectric function.

3. Results and discussion

In this section we present our results and discuss their implications. In Fig. 1, we show the variation of the density of impurity states (DOIS) of an on-center donor impurity in a cylindrical quantum well dot of axial length, $L_z = 10$ nm with binding energy for two different spatial dielectric functions when no uniaxial stress is applied. We observe that, for all spatial dielectric functions at a constant uniaxial length of the QD, the DOIS increases from some minimum and peaks in the low binding energy regime. There is then an almost exponential drop in DOIS to some minimum after which the DOIS then sharply rises almost exponentially to peak again in the high binding energy regime. The results for the DOIS for all the cases clearly show an important feature that is a peak at lower binding energies, which is the signature for QD structures. This is as a result of the contribution of impurities near the axial edge of the quantum well dot [29]. This effect becomes more pronounced as the dimensionality of the active layer is reduced making injected charge carriers to concentrate in an increasingly narrower energy range near the band edge.

Furthermore, it is quite noticeable that DOIS is higher when Hermanson's and linearized Thomas-Fermi spatial dielectric functions are applied than when a dielectric constant is used right from the onset of DOIS through their peaks. It has been observed in other works [29,30] that the dielectric function enhances donor binding energy. This means that the donor impurity becomes more tightly bound to its parent ion and, therefore, presents a larger DOIS profile than when the dielectric constant is used.

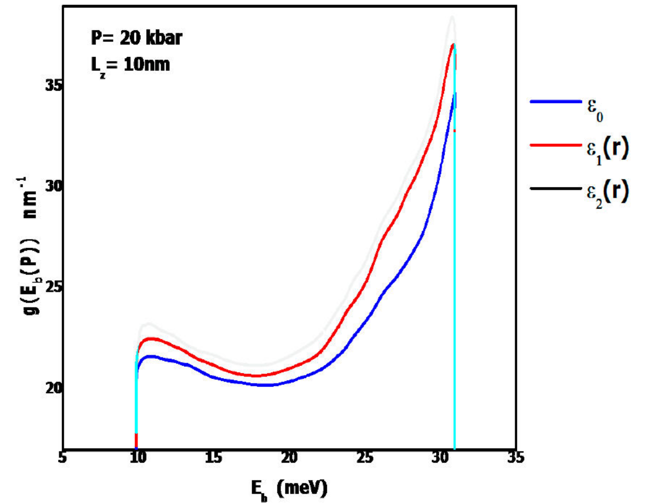

FIGURE 2. Density of impurity states (DOIS) of donor impurity in a cylindrical GaAs quantum well dot as a function of the donor binding energy at an applied uniaxial stress, $P = 20$ kbar for the dot's width $L_z = 10$ nm. ε_0, represents DOIS when dielectric constant is used, $\varepsilon_1(r)$ represents DOIS with Linearized Thomas-Fermi dielectric function, while $\varepsilon_2(r)$ represents DOIS with the Hermanson's spatial dielectric function.

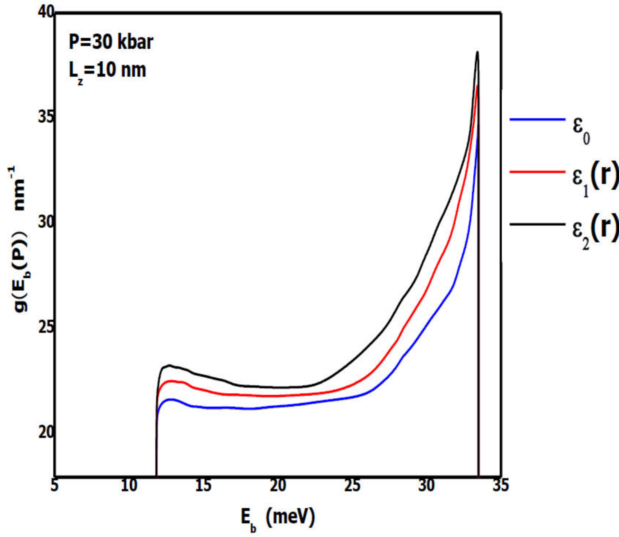

FIGURE 3. Density of impurity states (DOIS) of donor impurity in a cylindrical GaAs quantum well dot as a function of the donor binding energy at an applied uniaxial stress, $P = 30$ kbar for the dot's width $L_z = 10$ nm. ε_0 represents DOIS when dielectric constant is used, $\varepsilon_1(r)$ represents DOIS with Linearized Thomas-Fermi dielectric function, while $\varepsilon_2(r)$ represents DOIS with the Hermanson's spatial dielectric function.

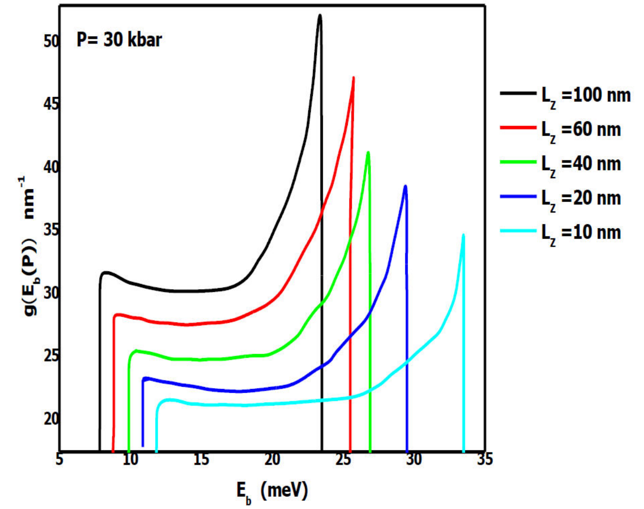

FIGURE 4. Density of impurity states (DOIS) of donor impurity in a cylindrical GaAs quantum well dot as a function of the donor binding energy at constant uniaxial stress, $P = 30$ kbar and for various quantum dot's lengths $L_z = 10$ nm, 20 nm, 40 nm, 60 nm and 100 nm when dielectric constant, ε_0 is used.

In Fig. 2, we show the variation of the DOIS of an on-center donor impurity in the quantum well dot of axial length, $L_z = 10$ nm with binding energy for the various spatial dielectric functions when a uniaxial stress of $P = 20$ kbar is applied. We have also observed, just like in Fig. 1, that all the peaks of the DOIS cluster around some range of binding energies. Thereafter, the DOIS decreases steeply at first and then gradually rises to a second peak at some higher values of binding energy. Essentially, we observe that the application of the uniaxial stress enhances the DOIS. The position of the first peak defines the minimum energy value of the laser required for the absorption in an experimental setup. The second peak in the DOIS, in the high-energy regime and with finite intensity, defines the resolution of the measurement system that identifies the structures in the spectra when the donor impurity is located away from the center of a QD [31]. In this sense, in the case of non-intentional doping, an almost defined structure should appear in the donor-related absorption spectra, located in the high energy range and associated to on-edge impurities.

In Fig. 3 shows variation of the DOIS of an on-center donor impurity in the QD with binding energy when the applied uniaxial stress is increased to $P = 30$ kbar. We have observed that a further increment in uniaxial stress displaces the DOIS towards higher energies. This is due to the increment of the dot effective masses as well as to the decreasing effect of dielectric screening and the barrier height with the stress [32,33]. On the other hand, the decrease of the dot size with increasing the uniaxial stress [32,33] results in a decrease of the effective electron-impurity distance leading to an increase in the DOIS profiles.

Finally in Fig. 4, we show the variation of the DOIS of an on-center donor impurity with binding energy in the QD for five various axial lengths, $L_z = 10$ nm, $L_z = 20$ nm, $L_z = 40$ nm, $L_z = 60$ nm and $L_z = 100$ nm, when the uniaxial stress is kept constant at $P = 30$ kbar. We have observed that the DOIS profiles for longer dots are larger and peak at lower binding energies than those for shorter ones. It would be interesting to check the results of the present study in an experimental work [34-36].

4. Conclusion

In the present work, we have performed a theoretical study of the effects of spatial dielectric functions and applied uniaxial stress on the density of impurity states (DOIS) of a donor impurity located at the center of a GaAs QD of circular cross-section. We have used a variational procedure within the effective mass approximation. We have found that the DOIS starts at particular value and sharply increases to a peak at low binding energy. This is then followed by a sharp and almost exponential drop in DOIS to some minimum after which the DOIS steeply rises to a second peak value in the high binding energy regime. The present work shows that, for constant axial length of the quantum dot and constant uniaxial stress, the DOIS for the non-hydrogenic donor impurity is markedly enhanced over that for purely hydrogenic donor impurity in which a dielectric constant is employed in the potential. Furthermore, we have seen that the uniaxial stress shifts the onset the DOIS to higher binding energy. The effect of the uniaxial stress seems to be the displacement of the DOIS towards higher energies. The present study indicates that the effects of spatial dielectric functions and uniaxial stress are important in the study of low-dimensional semiconductor systems such as QDs. Therefore, they should be considered in the

experimental studies of the electronic, optical and transport properties of such systems in order to improve device fabrication involving such nanostructures. It is expected that the results of the present work will stimulate the experimental study of the simultaneous effects of spatial dielectric functions and uniaxial stress on the donor impurity related optical absorption associated with shallow donor impurities in quantum well dots.

Acknowledgments

We would like to thank the registry of Partnerships, Research and Innovation (PRI) of Technical University of Mombasa for full financial support.

Author contributions

FO did all the analytical and numerical calculations besides writing the draft of the paper. HO originated the topic of the research, reviewed the analytical calculations and revised the initial draft of the paper.

Data availability statement

This manuscript has no associated data or the data will not be deposited. [Authors' comment: One can make reasonable request to the corresponding author in case of need of data in the present study. Furthermore, all the data can be readily generated using open-source code, by making use of the parameters listed in the text].

---

1. P. Harrison, and A. Valavanis, Quantum wells, wires and dots: Theoretical and Computational Physics of Semiconductor Nanostructures (John Wiley & Sons, Mroziewicz, B., 2016).
2. G. Bastard, Hydrogenic impurity states in a quantum well: A simple model, *Phys. Rev. B* **24** (1981) 4714, `https://doi.org/10.1103/PhysRevB.24.4714`.
3. W. T. Masselink, Yia-Chung Chang, and H. Morkoc, Binding energies of acceptors in GaAs-AlxGa1-xAs quantum wells, *Phys. Rev. B* **28** (1983) 7373, `https://doi.org/10.1103/PhysRevB.28.7373`.
4. P. Csavinszky and A. M. Elabsy, Dielectric response to a donor ion in a Ga1-xAlxAs-GaAs-Ga1-xAlxAs quantum well of infinite depth, *Phys. Rev. B* **32** (1985) 6498, `https://doi.org/10.1103/PhysRevB.32.6498`.
5. J. W. Brown and H. N. Spector, Hydrogen impurities in quantum well wires, *J. Appl. Phys.* **59** (1986) 1179, `https://doi.org/10.1063/1.336555`.
6. P. Csavinszky and H. Oyoko, Binding energy of on-axis hydrogenic and nonhydrogenic donors in a GaAs/Ga1-xAlxAs quantum-well wire of circularcross section, *Phys. Rev. B* **43** (1991) 9262, `https://doi.org/10.1103/PhysRevB.43.9262`.
7. A. Montes, C. A. Duque, and N. Porras-Montenegro, Density of shallowdonor impurity states in rectangular cross section GaAs quantum-well wires under applied electric field, *J. Phys.: Condens. Matter* **10** (1998) 5351, `https://doi.org/10.1088/0953-8984/10/24/012`.
8. H. Odhiambo Oyoko, C. A. Duque, and N. Porras-Montenegro, Theoretical study of the effect of applied stress on the binding energy of a donor impurity in GaAs quantum well dot within an infinite potential barrier, *Indian J. Pure and Appl. Phys.* **42** (2004) 908, `http://nopr.niscpr.res.in/handle/123456789/9648`.
9. A. Tiutiunnyk *et al.*, Electronic structure and optical properties of triangular GaAs/AlGaAs quantum dots: Exciton and impurity states, *Phys. B: Condens. Matter* **484** (2016) 95, `https://doi.org/10.1016/j.physb.2015.12.045`.
10. A. M. Elabsy, Hydrostatic pressure dependence of binding energies for donors in quantum well heterostructures, *Phys. Scr.* **48** (1993) 376, `https://doi.org/10.1088/0031-8949/48/3/019`.
11. A. L. Morales, A. Montes, S. Y. Lopez, and C. A. Duque, Simultaneous effects of hydrostatic stress and an electric field on donors in a GaAs-(Ga, Al)As quantum well, *J. Phys.: Condens. Matter* **14** (2002) 987, `https://doi.org/10.1088/0953-8984/14/5/304`.
12. S. Y. Lopez, N. Porras-Montenegro, and C. A. Duque, Binding energy and density of shallow impurity states in GaAs-(Ga,Al)As quantum wells: effects of an applied hydrostatic stress, *Semicond. Sci. Technol*. **18** (2003) 718, `https://doi.org/10.1088/0268-1242/18/7/322`.
13. N. Raigoza, A. L. Morales, A. Montes, N. Porras-Montenegro, and C. A. Duque, Stress effects on shallow-donor impurity states in symmetrical GaAs/AlxGa1-xAs double quantum wells, *Phys. Rev. B* **69** (2004) 045323, `https://doi.org/10.1103/PhysRevB.69.045323`.
14. N. Raigoza, A. L. Morales, and C. A. Duque, Effects of hydrostatic pressure on donor states in symmetrical GaAs-Ga0.7Al0.3As double quantum wells, *Phys. B: Cond. Matt.* **363** (2005) 262, `https://doi.org/10.1016/j.physb.2005.03.031`.
15. J. D. Correa, O. Cepeda-Giraldo, N. Porras-Montenegro, and C. A. Duque, Hydrostatic pressure effects on the donor impurity-related photoionization cross-section in cylindrical-shaped GaAs/GaAlAs quantum well wires, *Phys. Stat. Sol. (b)* **241** (2004) 3311, `https://doi.org/10.1002/pssb.200405225`.
16. E. Kasapoglu, H. Sari, M. Gunes, and I. Sökmen, The effect of hydrostatic pressure on optical transitions in quantum-well wires, *Phys. B: Cond. Matt.* **353** (2004) 345, `https://doi.org/10.1016/j.physb.2004.10.021`.
17. H. O. Oyoko, C. A. Duque, and N. Porras-Montenegro, Uniaxial stress dependence of the binding energy of shallow donor impurities in GaAs-(Ga,Al)As quantum dots, *J. Appl. Phys.* **90** (2001) 819, `https://doi.org/10.1063/1.1372976`.

18. A. J. Peter, The effect of hydrostatic pressure on binding energy of impurity states in spherical quantum dots, *Phys. E: Low-dim. Syst. and Nanostructures* **28** (2005) 225, https://doi.org/10.1016/j.physe.2005.03.018.

19. C. A. Duque, N. Porras-Montenegro, Z. Barticevic, M. Pacheco, and L. E. Oliveira, Electron-hole transitions in self-assembled InAs/GaAs quantum dots: Effects of applied magnetic fields and hydrostatic pressure, *Microelectronics Journal* **36** (2005) 231, https://doi.org/10.1016/j.mejo.2005.04.001.

20. H. Oyoko, Effect of Hermanson's spatial dielectric function on donor impurity binding energy in a cylindrical cross-sectional GaAs/GaAlAs quantum well wires on infinite length, *Indian J. Pure and Appl. Phys*. **38** (2000) 512, http://nopr.niscpr.res.in/handle/123456789/26911.

21. F. Oketch and H. Oyoko, A theoretical study of variation of photoionization cross section of donor impurities in a GaAs quantum dot of cylindrical geometry with incident photon frequency, donor location along the dot axis and applied uniaxial stress, *Rev. Mex. Fis*. **66** (2020) 35, https://doi.org/10.31349/revmexfis.66.35.

22. F. Oketch and H. Oyoko, A theoretical study of the effects of Thomas-Fermi and Hermanson's dielectric functions and temperature on photoionization crosssection of a donor impurity in GaAs quantum dots of circular and rectangular cross-sections, *Eur. Phys. J. B* **95** (2022) 44, https://doi.org/10.1140/epjb/s10051-022-00301-4.

23. F. Oketch, H. Oyoko and G. Amolo, A Study of the Effect of Hermanson's Spatial Dielectric Function on the Photoionization Cross-Section of a Hydrogenic and a non-Hydrogenic Donor Impurity in a GaAs Quantum Dot of Cylindrical Geometry in the Region of Finite and Infinite Barrier Potentials, *J. Korean Phys. Soc.* **73** (2018) 928, https://doi.org/10.3938/jkps.73.928.

24. J. D. Correa, N. Porras-Montenegro and C. A. Duque, Donor-related photoionization cross-section of GaAs-(Ga, Al)As quantum dots: hydrostatic pressure effects, *Phys. stat. sol. (b)* **241** (2004) 2440, https://doi.org/10.1002/pssb.200404908.

25. B. Welber, M. Cardona, C. K. Kim, and S. Rodriguez, Dependence of the direct energy gap of GaAs on hydrostatic pressure, *Phys. Rev. B* **12** (1975) 5729, https://doi.org/10.1103/PhysRevB.12.5729.

26. D. E. Aspnes, GaAs lower conduction-band minima: Ordering and properties, *Phys. Rev. B* **14** (1976) 5331, https://doi.org/10.1103/PhysRevB.14.5331.

27. S. Adachi, GaAs, AlAs, and AlxGa1-xAs: Material parameters for use in research and device applications, *J. Appl. Phys.* **58** (1985) R1, https://doi.org/10.1063/1.336070.

28. M. E. Mora-Ramos, S. Y. Lopez and C. A. Duque, $\Gamma - X$ mixing in GaAs- Ga1-xAlxAs quantum wells under hydrostatic pressure, *Eur. Phys. J. B* **62** (2008) 257, https://doi.org/10.1140/epjb/e2008-00161-6.

29. H. Odhiambo Oyoko, The Effect of Uniaxial Stress on the Density of States of Shallow Donor Impurities in GaAs Quantum Wells, *Phys. Scr.* **66** (2002) 94, https://doi.org/10.1238/Physica.Regular.066a00094.

30. P. Csavinszky and H. Oyoko, Binding energies of on-axis hydrogenic and nonhydrogenic donors in GaAs/Ga1-x AlxAs, *Journal of Mathematical Chemistry* **9** (1992) 197, https://doi.org/10.1007/BF01165147.

31. H. Odhiambo Oyoko, N. Porras-Montenegro, S. Y. Lopez and C. A. Duque, Comparative study of the hydrostatic pressure and temperature effects on the impurity-related optical properties in single and double GaAs-Ga1-x AlxAs quantum wells, *Phys. stat. sol(c)* **4** (2007) 298, https://doi.org/10.1002/pssc.200673259.

32. A. Sivakami, M. Mahendran, Hydrostatic pressure and conduction band non-parabolicity effects on the impurity binding energy in a spherical quantum dot, *Phys. B: Cond. Matt.* **405** (2010) 1403, https://doi.org/10.1016/j.physb.2009.12.008.

33. A. Sivakami, V. Gayathri, Hydrostatic pressure and temperature dependence of dielectric mismatch effect on the impurity binding energy in a spherical quantum dot, *Superlatt. Microstruct.* **58** (2013) 218, https://doi.org/10.1016/j.spmi.2013.03.002.

34. X. Hu *et al*., Photoluminescence of InAs/GaAs quantum dots under direct twophoton excitation, *Sci. Rep.* **10** (2020) 10930, https://doi.org/10.1038/s41598-020-67961-z.

35. S. Zhu, Y. Song, X. Zhao, J. Shao, J. Zang, and B. Yang, The photoluminescence mechanism in carbon dots (graphene quantum dots, carbon nanodots, and polymer dots): Current state and future perspective, *Nano Res.* **8** (2015) 355, https://doi.org/10.1007/s12274-014-0644-3.

36. F. Liu *et al*., Highly Luminescent Phase-Stable CsPbI3 Perovskite Quantum Dots Achieving Near 100% Absolute Photoluminescence Quantum Yield, *ACS Nano* **11** (2017) 10373, https://doi.org/10.1021/acsnano.7b05442.